Disaggregation of SMAP L3 Brightness Temperatures to 9km using Kernel Machines

Subit Chakrabarti, *Student Member, IEEE*, Tara Bongiovanni, Jasmeet Judge, *Senior Member, IEEE*, Anand Rangarajan, *Member, IEEE*, Sanjay Ranka, *Fellow, IEEE*.

Abstract

In this study, a novel machine learning algorithm is presented for disaggregation of satellite brightness $\mathrm{T_B}$ observations from 36km to 9km. It uses a segmentation step that divides the study region into regions based on meteorological and land cover similarity, followed by a support vector machine based regression that computes the value of the disaggregated $\mathrm{T_B}$ at all pixels. Coarse-scale remotely sensed $\mathrm{T_B}$ were disaggregated from 36km to 9km using land surface temperature, normalized difference vegetation index, enhanced vegetation index, precipitation, soil texture and land-cover. This algorithm was implemented in Iowa in the United states during May to August 2015 and validated using the SMAP L3_SM_AP $\mathrm{T_B}$ product at 9km. It was found that the disaggregated $\mathrm{T_B}$ were very similar to the L3_SM_AP $\mathrm{T_B}$ product, even for highly vegetated areas. The difference between the means of the disaggregated $\mathbf{T_B}$ and L3_SM_AP $\mathbf{T_B}$ were $\leq$ 5K for all days while the variances were 7K lower on average. The probability density functions of the disaggregated $\mathrm{T_B}$ and L3_SM_AP $\mathrm{T_B}$ were found to be alike. The results indicate that this algorithm can be used for disaggregating $\mathrm{T_B}$ with complex non-linear correlations on a grid with high accuracy and can be used as a substitute for the SMAP L3_SM_AP $\mathrm{T_B}$ product.

Index Terms

Disaggregation, Microwave Remote Sensing, Soil Moisture, Kernel Regression, Clustering, Multi-spectral Remote Sensing.

This work was supported in part by the NASA-Terrestrial Hydrology Program (THP)-NNX13AD04G.

S. Chakrabarti and J. Judge are with the Center for Remote Sensing, Agricultural and Biological Engineering Department, Institute of Food and Agricultural Sciences, University of Florida, Gainesville, USA; A. Rangarajan and S. Ranka are with the Department of Computer & Information Science & Engineering, University of Florida, Gainesville. E-mail: subitc@ufl.edu

A version of this manuscript has been submitted to IEEE Geoscience and Remote Sensing Letters.

I. Introduction

Satellite based microwave observations are highly sensitive to near-surface soil moisture (SM) [1]–[10]. The NASA Soil Moisture Active and Passive (SMAP) mission was expected to provide SM at a spatial resolution of 9 km retrieved from combined active and passive (AP) observations at 1.26 and 1.41 GHz, respectively, every 2-3 days [11]. This spatial resolution is needed for many hydrometeorological applications [12]–[18]. However, on July 7th 2015, the radar on board SMAP halted its transmissions due to an anomaly [19], creating a significant gap in the disaggregation of coarse scale radiometer observations (T_B) available at 36km to 9km to meet the mission requirements for the L3_SM_AP product. A few studies have attempted to disaggregate T_B directly without the complementary information provided by active observations. Statistical inversion techniques such as linear inversion with regularization [20], singular value decomposition (SVD) [21] and, gradient descent in Banach spaces [22] have been used for this purpose. These techniques allow discovery of non-linear correlations between T_B across scales. However, these methods require a training set of high-resolution T_B, which is not typically available. Piles et. al. [23] disaggregated T_B directly into SM by applying the Universal Triangle (UT) method and used a second-degree regression-based linking model to relate coarse resolution SM to T_B from the SMOS mission, and other high resolution products, aggregated to the resolution of SMOS observations. The fine scale SM was then estimated using the assumption that the linking model at the coarse resolution also holds at finer resolutions. The robustness of this method over heterogeneous vegetation and weather conditions remain mostly untested. Treating each pixel as a sample instead of using spatial information to regularize the disaggregation results in salt and pepper noise due to spatial auto-correlation [24]. Moreover, these approaches use second order metrics, which do not leverage all the information in the data that is necessary in a highly non-linear regression problem such as disaggregation [25].

The goal of this study is to enhance the SRRM algorithm [26] to disaggregate T_B using kernel based support vector regression models and spatial segmentation. The segmentation algorithm separates the study region into discrete sets of pixels which have similar land-cover and micro-meteorological conditions. A support vector regression model is estimated for each set using coarse scale T_B and auxiliary correlated data which is further applied to the auxiliary data at fine scale to obtain disaggregated T_B. The primary objectives are to, 1) modify the SRRM algorithm to downscale SMAP T_B to 10 km using other spatially correlated variables such as land surface temperature(LST), normalized difference vegetation index (NDVI), enhanced vegetation index (EVI), precipitation (PPT), soil texture and land-cover (LC), 2) implement the downscaling algorithm in Iowa in mid-western United States, and 3) validate the performance of the algorithm by comparing the disaggregated T_B to the SMAP L3_SM_AP T_B during May to August, 2015 when the SMAP radar observations were available.

II. Theory

Disaggregation is an ill-posed problem constrained by the smoothness of the coarse-scale data which constrains the generation of data at fine scale because any added sharpness can be misconstrued as noise. Additional geospatial and meteorological data that are correlated to T_B are needed to ensure that the added sharpness has physical basis. In this study, these auxiliary data-sets are utilized to create localized regression models that provide a mapping from the T_B at coarse scale to T_B at fine scale. To ensure that the localization is realistic and not arbitrary, the coarse T_B image is first segmented into multiple regions of radiometric similarity. The overall organization and the datasets involved is shown in Figure 1.

A. Self-Regularized Regressive Models (SRRM)

The *first step* of the algorithm divides the study area into segments using the coarse scale T_B. In this study, the segmentation algorithm uses information theoretic measures of inter and intra segment similarity [27]. If $\mathbf{X} = \{\mathbf{x}_1, \mathbf{x}_2, \mathbf{x}_3 \ldots \mathbf{x}_N\}$ is a matrix containing T_B for N pixels, the Cauchy-Schwarz cost-function, $\hat{J}_{CS}$, estimates optimal memberships of the pixels to segments, $\mathbf{m}$, in an un-supervised manner.

$$\hat{J}_{CS}^{REG} = \frac{\frac{1}{2}\sum_{i=1}^{N}\sum_{j=1}^{N}\left(1-\mathbf{m}_i^{\mathrm{T}}\mathbf{m}_j\right)G_{\sigma\sqrt{2}}\left(\mathbf{x}_i,\mathbf{x}_j\right)}{\sqrt{\prod_{k=1}^{K}\sum_{i=1}^{N}\sum_{j=1}^{N} m_{ik}m_{jk}G_{\sigma\sqrt{2}}(\mathbf{x}_i,\mathbf{x}_j)}} \tag{1}$$

where, K is the number of segments, $G_{\sigma\sqrt{2}}$ is the Gaussian kernel with standard-deviation σ and ν is the regularization weight. The optimal value of the membership vector can be obtained from the following constrained optimization problem,

$$\begin{aligned}&\min_{\mathbf{m}_1,\ldots,\mathbf{m}_N} \hat{J}_{CS}^{REG}(\mathbf{m}_1,\ldots,\mathbf{m}_N)\\ &\text{subject to } \mathbf{m}_j^{\mathrm{T}}\mathbf{1}-\mathbf{1}=0, \quad j=1,\ldots,N\end{aligned} \tag{2}$$

To compute optimum values of $\mathbf{m}$, and thus the membership of each pixel to the K segments, a Lagrange multiplier formulation can be used along with a stochastic gradient descent scheme, the details of which are shown in [26].

In the *second step*, support vector regression(SVR) [28], is used to generate the downscaled estimates. A training set of pixels, for example y_{train} is used in the regression to fit a non-linear function, for example f, from the set of the auxiliary data and coarse scale $\mathrm{T_B}$, for example $\mathbf{z}$, to fine scale $\mathrm{T_B}$. This function takes the form,

$$f(z) = < w, z >_{\mathcal{H}} + b \tag{3}$$

where w are the weights and $< ., . >$ is the inner-product operation in some Hilbert space, $\mathcal{H}$. The cost function of support vector regression, which minimizes the errors between y_{train} and $f(z)$ to at most ϵ,

$$\frac{1}{2}\|w^2\| + C\sum_{i=1}^{l}(\xi_i+\xi_i^*) \tag{4}$$

$$\text{subject to } \begin{cases} y_{train} - < w, z >_{\mathcal{H}} - b \leq \epsilon + \xi_i \\ < w, z >_{\mathcal{H}} + b - y_{train} \leq \epsilon + \xi_i^* \\ \xi_i^*, \xi_i \geq 0 \end{cases}$$

where ξ_i^* and ξ_i are called *slackness constants* such that Equation 4 can be solved using convex optimization and C determines the trade-off between the flatness of f and the amount up to which deviations greater that ϵ are tolerated. The function f is allowed to be non-linear by selecting a suitable $\mathcal{H}$ such that the inner product becomes a kernel evaluation as $< w, z >_{\mathcal{H}} = \kappa(w, z)$. In this study the radial basis function kernel was chosen, $\kappa(w,z) = \exp\left(\frac{\|w-z\|^2}{2\sigma^2}\right)$ where σ is the kernel parameters. More details about the statistics and convex optimization theory that is used to solve SVR based problems are available in [29], [30] and are not repeated here.

III. Experimental Description and Results

A. Study Area

The study was conducted in a 320×560 km^2 region in the state of Iowa in the United States (US), stretching from $40.36°$ to $43.57°$N and $90.14°$ to $96.68°$W, equivalent to 162 SMAP pixels. Iowa with an area of about 1.7×10^5 km^2, out of which 1.2×10^5 km^2 is cropland, is one of the most important agricultural areas in the US responsible for $> 70\%$ of the country's agricultural gross domestic product [31]. The region is a major agricultural region of economic importance for the US. The primary agricultural land covers in the region are corn and soybean accounting for over 90% of agricultural land covers. Agricultural areas with other crops were conglomerated and referred to as 'miscellaneous' in this study. Some forests, wetlands and developed regions were also present in the study area. The ratio of each land-cover within a single 1-km pixel is shown in Figure 2(a) through (f). The percentage of silt, clay and soil is also shown in the study region in Figure 3.

To downscale SMAP SM at 36 km to 9 km, satellite based observations of EVI, NDVI, LST, PPT were used from April 20$^{\text{th}}$ to June 30$^{\text{th}}$ 2015. LC and soil texture were also used and considered to be constant for the duration of the study. The satellite-based observations used in this study along with their spatio-temporal resolutions are listed in Table I. The 3-hour PPT data was averaged over a three day time period using a moving window to obtain 3-day averaged PPT.

B. Implementation in Iowa

In the first step of the modified SRRM algorithm, the D_{CS} based clustering algorithm to discover regions of similarity in the study area. In Equation 1, $\mathbf{X} = \{[\mathrm{T_{B,1}}, \mathrm{lat}_1, \mathrm{lon}_1], [\mathrm{T_{B,1}}, \mathrm{lat}_2, \mathrm{lon}_2], \ldots, [\mathrm{T_{B,M}}, \mathrm{lat}_M, \mathrm{lon}_M]\}$ where M is the total number of coarse pixels in the region and $\mathrm{lat_i}$ and $\mathrm{lon_i}$ are the latitude and longitude of the i^{th} pixel. This step of the algorithm uses one parameter - the number of clusters, N. Since no ground truth is available in the region, N cannot be determined using cross-validation as used in the SRRM algorithm [26]. Instead the principle of minimum description length as described in [32] is used.

In the second step of the algorithm, M models, $\hat{f}_1, \hat{f}_2, \ldots, \hat{f}_M$ are developed using NDVI, EVI, PPT, LST, LC and soil texture aggregated to 36km along with the coarse scale $\mathrm{T_B}$ using Equation 4. The disaggregated value of SM at 9km is then computed by applying the learnt functions $\hat{f}_1, \hat{f}_2, \ldots, \hat{f}_M$ to NDVI, EVI, PPT, LST and LC values aggregated to 9km.

The means and standard deviations of the disaggregated $\mathrm{T_B}$ and L3_SM_AP $\mathrm{T_B}$ are compared for each day of the study to provide an index of the amount of variability captured in the $\mathrm{T_B}$. The downscaling algorithm is further evaluated by comparing the disaggregated $\mathrm{T_B}$ to the L3_SM_AP product, also available at 9km, for three days during the study with disparate levels of vegetation and precipitation. To determine the relationship between the disaggregated $\mathrm{T_B}$ and coarse scale SMAP $\mathrm{T_B}$ at 36km, and compare this with the relationship between the L3_SM_AP $\mathrm{T_B}$ and coarse scale SMAP $\mathrm{T_B}$, the probability density function of the three products are estimated and used.

Figure 4 shows the means and standard deviations of the disaggregated $\mathrm{T_B}$ and L3_SM_AP $\mathrm{T_B}$ for each day of the study. The means are preserved by the multiscale SRRM algorithm with differences of $\leq$ 0.5K while the standard-deviations of the disaggregated $\mathrm{T_B}$ is, on an average 7K lower than for the L3_SM_AP $\mathrm{T_B}$. This is due to the absence of radar noise in the disaggregated $\mathrm{T_B}$, as is evident in Figure 5 which shows the the disaggregated $\mathrm{T_B}$ and inputs for DoY 125 of the study. Although the major variability in the inputs and L3_SM_AP $\mathrm{T_B}$ are present in the disaggregated $\mathrm{T_B}$, it is also smoother compared to L3_SM_AP $\mathrm{T_B}$ which suggests low noise levels. Similar performance is observed for DoYs 157 and 181, shown in Figure 6 and Figure 7 respectively. The locations of the clusters also change appropriately on both the days according to the spatial patters of $\mathrm{T_B}$. Furthermore, even when the NDVI and EVI is high, as observed for DoY 181, the disaggregated $\mathrm{T_B}$ is accurate as compared to the L3_SM_AP $\mathrm{T_B}$. Thus, the multiscale SRRM algorithm is sufficiently robust to vegetation levels and landcovers. The statistical similarity of disaggregated $\mathrm{T_B}$ to the coarse scale SMAP $\mathrm{T_B}$ is shown in Figure 8. The PDF of disaggregated $\mathrm{T_B}$ is closer to the PDF of coarse scale SMAP $\mathrm{T_B}$ than the L3_SM_AP $\mathrm{T_B}$ which shows that the disaggregated $\mathrm{T_B}$ is more closely coupled to the coarse scale SMAP $\mathrm{T_B}$. This demonstrates that the multi-scale SRRM algorithm can be operationally used to disaggregate the coarse scale SMAP $\mathrm{T_B}$ to 9 km and act as a good substitute for the L3_SM_AP $\mathrm{T_B}$ product.

IV. Conclusion

In this study, a disaggregation methodology from 36km to 9km was developed and implemented that preserves the high variability in $\mathrm{T_B}$ due to heterogeneous meteorological and vegetation conditions. The multiscale SRRM preserves heterogeneity by utilizing a segmentation algorithm to create a number of regions of similarity which subsequently, are used in a support vector machine regression framework. The clusters were computed using RS products, *viz.* PPT, EVI, NDVI, LC and Soil Texture. It was found that the difference between the means of the disaggregated $\mathrm{T_B}$ and L3_SM_AP $\mathrm{T_B}$ is $\leq$ 5K for all days while the variances are 7K lower on average. The disaggregated $\mathrm{T_B}$ and L3_SM_AP $\mathrm{T_B}$ were alike even under highly vegetated conditions. The PDFs of the disaggregated $\mathrm{T_B}$ were found to be closer to the PDF of the coarse scale SMAP $\mathrm{T_B}$ than the PDF of L3_SM_AP $\mathrm{T_B}$ product. The results indicate that this algorithm can be used for disaggregating $\mathrm{T_B}$ with complex non-linear correlations on a grid with high accuracy and can be used as a substitute for the SMAP L3_SM_AP $\mathrm{T_B}$ product.

References

[1] J. T.J and T. Schmugge, "Vegetation effects on the microwave emission of soils," *Remote Sens. Env.*, vol. 36, no. 3, pp. 203–212, 1991.
[2] T. Jackson and T. Schmugge, "Surface soil moisture measurement with microwave radiometry," *Acta Astronautica*, vol. 35, no. 7, pp. 477–482, 1995.
[3] S. Ahmad, A. Kalra, and H. Stephen, "Estimating soil moisture using remote sensing data: A machine learning approach," *Adv. in Water Res.*, vol. 33, pp. 69–80, 2010.
[4] C. Gruhier, P. de Rosnay, S. Hasenauer, T. Holmes, R. de Jen, Y. Kerr, E. Mougin, E. Njoku, F.Timouk, W. Wagner, and M. Zribi, "Soil moisture active and passive microwave products: intercomparison and evaluation over a Sahelian site," *Hydrology and Earth System Sciences*, vol. 14, pp. 141–156, 2010.
[5] B. W. Barrett, E. Dwyer, and P. Whelan, "Soil moisture retrieval from active spaceborne microwave observations: an evaluation of current techniques," *Remote sensing*, vol. 1, pp. 210–242, 2009.
[6] J. Qin, S. Liang, K. Yang, I. Kaihotsu, R. Liu, and T. Koike, "Simultaneous estimation of both soil moisture and model parameters using particle filtering method through the assimilation of microwave signal," *Journal of Geophysical Research*, vol. 114, p. doi:10.1029/2008JD011358, 2009.
[7] T. Lakhankar, N. Krakauer, and R. Khanbilvardi, "Applications of microwave remote sensing of soil moisture for agricultural applications," *International Journal of Terraspace Science and Engineering*, vol. 2, no. 1, pp. 81–91, 2009.
[8] K. B. Mao, H. J. Tang, L. X. Zhang, M. C. Li, Y. Guo, and D. Z. Zhao, "A method for retrieving soil moisture in Tibet region by utilizing microwave index from TRMM/TMI data," *Int. J. Remote Sensing*, vol. 29, no. 10, pp. 2903–2923, 2008.
[9] L. Wang, J. J. Qu, S. Zhang, X. Hao, and S. Dasgupta, "Soil moisture retrieval using EOS MODIS and ground measurements in Eastern China," *Int. J. Remote Sensing*, vol. 28, no. 6, pp. 1413–1418, 2007.
[10] S. Dongsheng, Z. Kai, and G. Zhi, "Advances in research on soil moisture by microwave remote sensing in china," *Chinese Geographical Science*, vol. 17, no. 2, pp. 186–191, 2007.
[11] D. Entekhabi, E. Njoku, P. O'Neill, M. Spencer, T. Jackson, J. Entin, E. Im, and K. Kellogg, "The Soil Moisture Active/Passive Mission (SMAP)," in *IEEE Int. Geosc. and Rem. Sens. Symposium*, vol. 3. Proc. IGARSS 2008, 2008, pp. III–1 – III–4.
[12] M. Fennessy and J. Shukla, "Impact of initial soil wetness on seasonal atmospheric prediction," *J. Clim.*, vol. 12, pp. 3167–3180, 2009.
[13] H. Douville and F. Chauvin, "Relevance of soil moisture for seasonal climate predictions: A preliminary study," *Clim. Dyn.*, vol. 16, pp. 719–736, 2000.
[14] The GLACE Team, R. Koster1, P. Dirmeyer, Z. Guo, G. Bonan, E. Chan, P. Cox, C. Gordon, S. Kanae, E. Kowalczyk, D. Lawrence, P. Liu, C. Lu, S. Malyshev, B. McAvaney, K. Mitchell, D. Mocko, T. Oki, K. Oleson, A. Pitman, Y. Sud, C. Taylor, D. Verseghy, R. Vasic, Y. Xue, and T. Yamada, "Regions of strong coupling between soil moisture and precipitation," *Science*, vol. 305, no. 5687, pp. 1138–1140, 2004.
[15] F. Tubiello, C. Rosenzweig, R. Goldberg, S. Jagtap, and J. Jones, "Effects of climate change on U.S. crop production: Simulation results using two different GCM scenarios. part i: Wheat, potato, maize, and citrus," *Clim. Res.*, vol. 20, pp. 259–270, 2002.
[16] J. Yuste, M. Nagy, I. Jenkins, I. Janssens, A. Carrara, and R. Ceulemans, "Soil respiration in a mixed temperate forest and its contribution to total ecosystem respiration," *Tree Physiol.*, vol. 25, no. 05, pp. 609–619, 2005.
[17] A. Friend, A. Arneth, N. Kiang, M. Lomass, J. Ogee, C. Rodenbeck, S. Running, J. Santaren, S. Sitch, N. Viovy, F. Woodwards, and S. Zaehle, "FLUXNET and modelling the global carbon cycle," *Global Change Biology*, vol. 13, pp. 613–633, 2007.
[18] F. Fecan, B. Marticorena, and G. Bergametti, "Parametrization of the increase of the aeolian erosion threshold wind friction velocity due to soil moisture for arid and semi-arid areas," *Ann. Geophys.-Atmos. Hydrospheres Space Sci.*, vol. 17, no. 01, pp. 149–157, 1999.
[19] NASA SMAP Team. (2015) NASA soil moisture radar ends operations, mission science continues. [Online]. Available: http://smap.jpl.nasa.gov/news/1247/
[20] Y. Wang, J. Shi, L. Jiang, J. Du, and B. Tian, "The development of an algorithm to enhance and match the resolution of satellite measurements from amsr-e," *Science China: Earth Sciences*, vol. 54, no. 3, pp. 410–419, 2011.
[21] A. Gambardella and M. Migliaccio, "On the superresolution of microwave scanning radiometer measurements," *IEEE Geosci. and Remote Sensing Letters*, vol. 5, no. 4, pp. 796–800, 2008.
[22] F. Lenti, F. Nunziata, C. Estatico, and M. Migliaccio, "On the spatial resolution enhancement of microwave radiometer data in banach spaces," *IEEE Trans. Geosci. Remote Sensing*, vol. 52, no. 3, pp. 1834–1842, 2014.
[23] M. Piles, M. Vall-llossera, L.Laguna, and A. Camps, "A downscaling approach to combine SMOS multi-angular and full-polarimetric observations with mdis vis/ir data into high resolution soil moisture maps," in *IEEE Int. Geosc. and Rem. Sens. Symposium*, vol. 1. Proc. IGARSS 2012, 2012, pp. 1247–1250.
[24] Z. Jiang, S. Shekhar, X. Zhou, J. Knight, and J. Corcoran, "Focal-test-based spatial decision tree learning: A summary of results," *Proceedings of the IEEE 13th International Conference on Data Mining (ICDM)*, pp. 320–329, 2013.
[25] J. Principe, D. Xu, and J. Fisher, *Information theoretic learning, in unsupervised adaptive filtering*. New York: Wiley, 2010.

[26] S. Chakrabarti, J. Judge, A. Rangarajan, and S. Ranka, “Disaggregation of remotely sensed soil moisture in heterogeneous landscapes using holistic structure based models,” *IEEE Trans. Geosci. Remote Sensing*, vol. Under Review, 2015.
[27] R. Jennsen, D. Erdogmus, K. Hild, J. Principe, and T. Eltoft, “Optimizing the Cauchy-Schwarz PDF distance for information theoretic, non-paremetric clustering,” in *Proceedings of the 5th international conference on Energy Minimization Methods in Computer Vision and Pattern Recognition*, vol. 1. Proc. EMMCVPR 2005, 2005, pp. 34–45.
[28] V. Vapnik, S. Golowich, and A. Smola, “A tut,” *Advances in Neural Information Processing*, vol. 9, pp. 281–287, 1996.
[29] A. Smola and B. Schölkopf, “A tutorial on support vector regression,” *Statistics and Computing*, vol. 14, pp. 199–222, 2004.
[30] S. Clarke, J. Griebsch, and T. Simpson, “Analysis of support vector regression for approximation of complex engineering analyses,” *J. Mech. Des*, vol. 127, no. 6, pp. 1077–1087, 2004.
[31] T. Vilsack and C. Clark, “Census of agriculture - United States,” National Agricultural Statistics Service, Washington, DC, Tech. Rep., 2012.
[32] M. Hanse and B. Yu, “Model selection and the principle of minimum description length,” *Journal of the American Statistical Association*, vol. 96, no. 454, pp. 746–774, 2001.

TABLE I
SATELLITE OBSERVATIONS

Sl. No.	Physical Quantity	Original Resolution	Interpolated Resolution (km)	Source	Temporal Resolution
1	Brightness Temperature	36 km	-	NASA-SMAP	2-3 days
2	Precipitation	0.1°	1	NASA-GPM	30 min
3	Enhanced Vegetation Index	1 km	-	NASA Aqua/Terra (MODIS)	8 days
4	Land Surface Temperature	1 km	-	NASA Aqua/Terra (MODIS)	1 day
5	Land Cover	30 m	1 km	USDA NASS-CDL	1 year
6	Normalized Difference Vegetation Index	0.125°	1	NASA Aqua/Terra (MODIS)	8 days

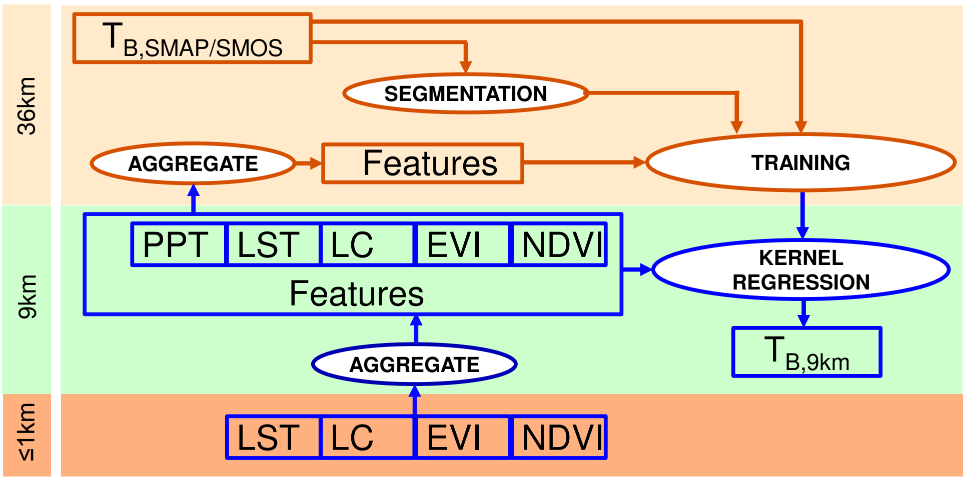

Fig. 1. Flowchart for the multi-scale SRRM disaggregation method.

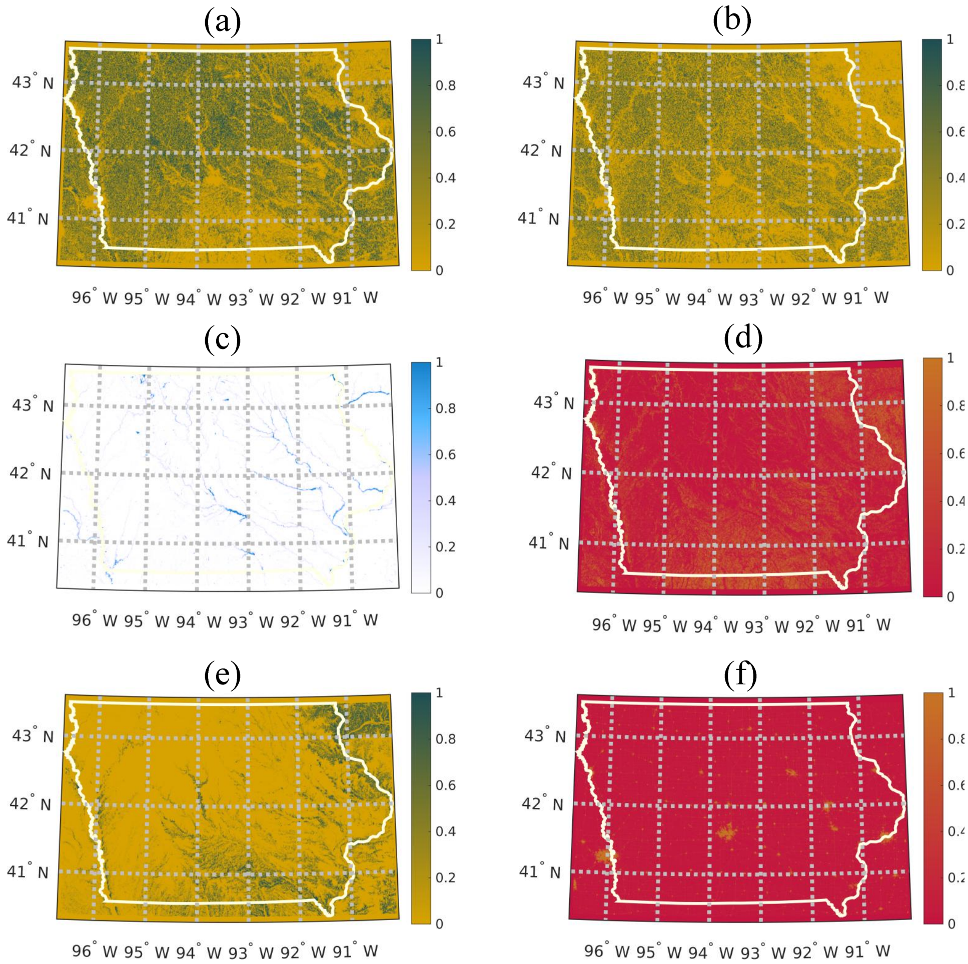

Fig. 2. Land Covers in the study region in Iowa, United States - (a) Corn, (b) Soybean, (c) Water, (d) Other, (e) Forest, (f) Miscellaneous.

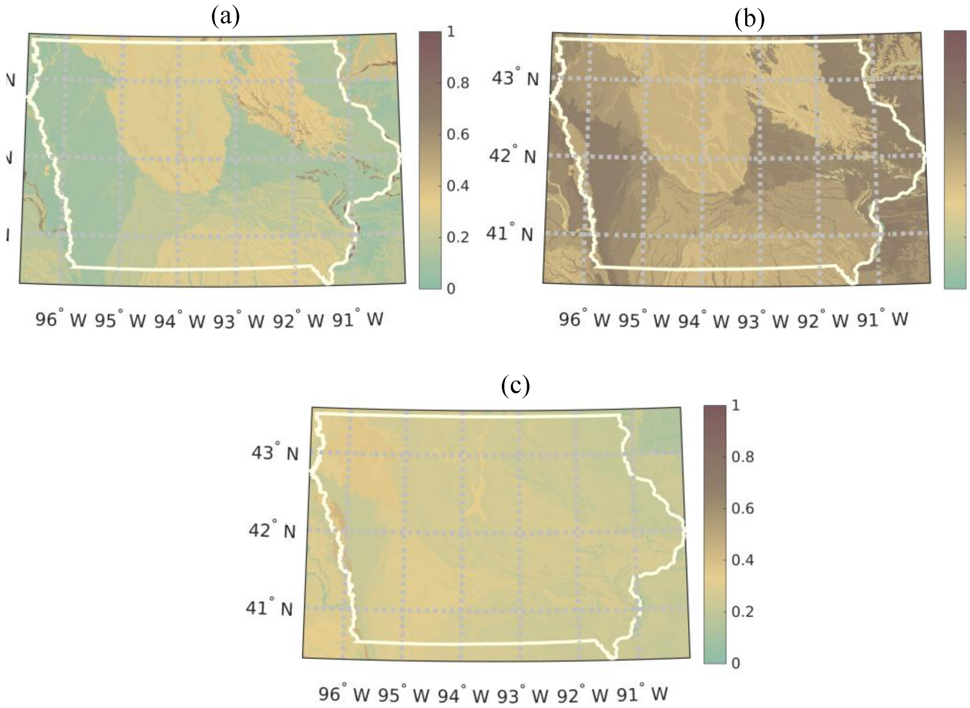

Fig. 3. Soil texture in the study region in Iowa, United States - ratio of (a)sand, (b)clay and (c)silt in the soil.

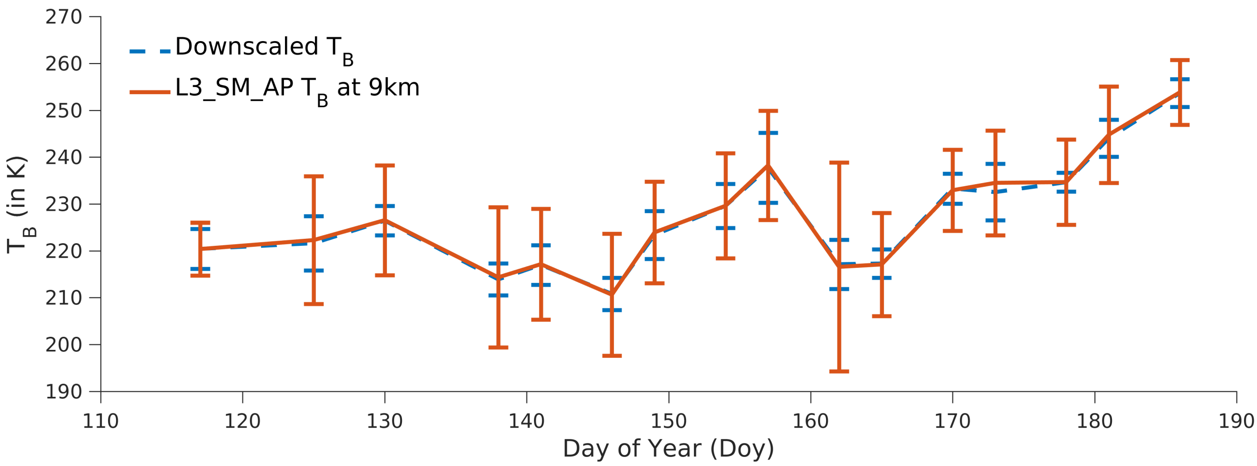

Fig. 4. Spatial average and variance of disaggregated brightness temperature and SMAP L3_SM_AP product at 9km for the whole season.

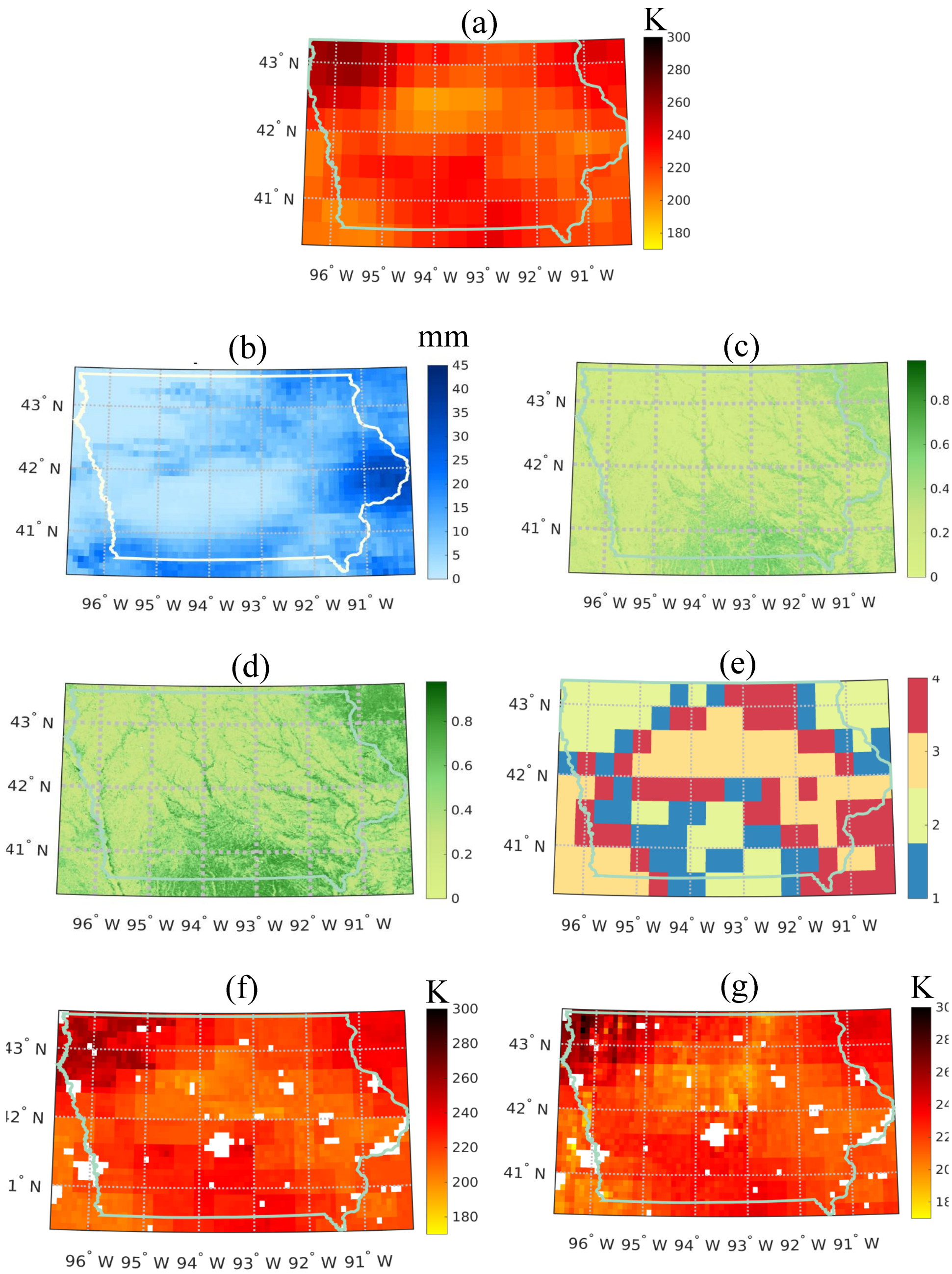

Fig. 5. DoY 125 - (a) SMAP L1C_TB product at 36km, (b) Precipitation at 1km, (c) Normalized Difference Vegetation Index at 1km, (d) Enhanced vegetation index at 1km, (e) Segmentation at 36km, (f) Disaggregated brightness temperature at 9km, (g) SMAP L3_SM_AP product at 9km.

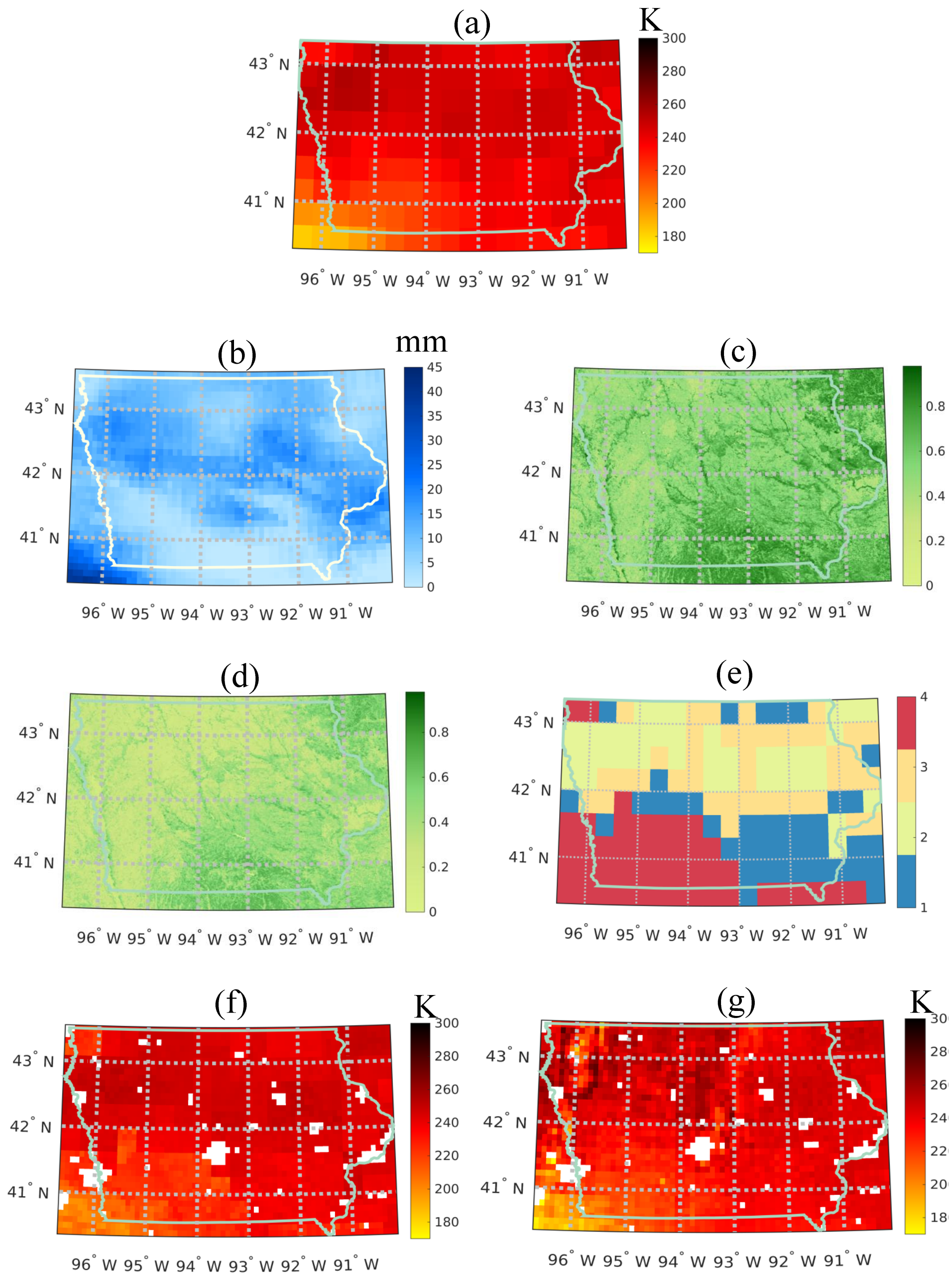

Fig. 6. DoY 157 - (a) SMAP L1C_TB product at 36km, (b) Precipitation at 1km, (c) Normalized Difference Vegetation Index at 1km, (d) Enhanced vegetation index at 1km, (e) Segmentation at 36km, (f) Disaggregated brightness temperature at 9km, (g) SMAP L3_SM_AP product at 9km.

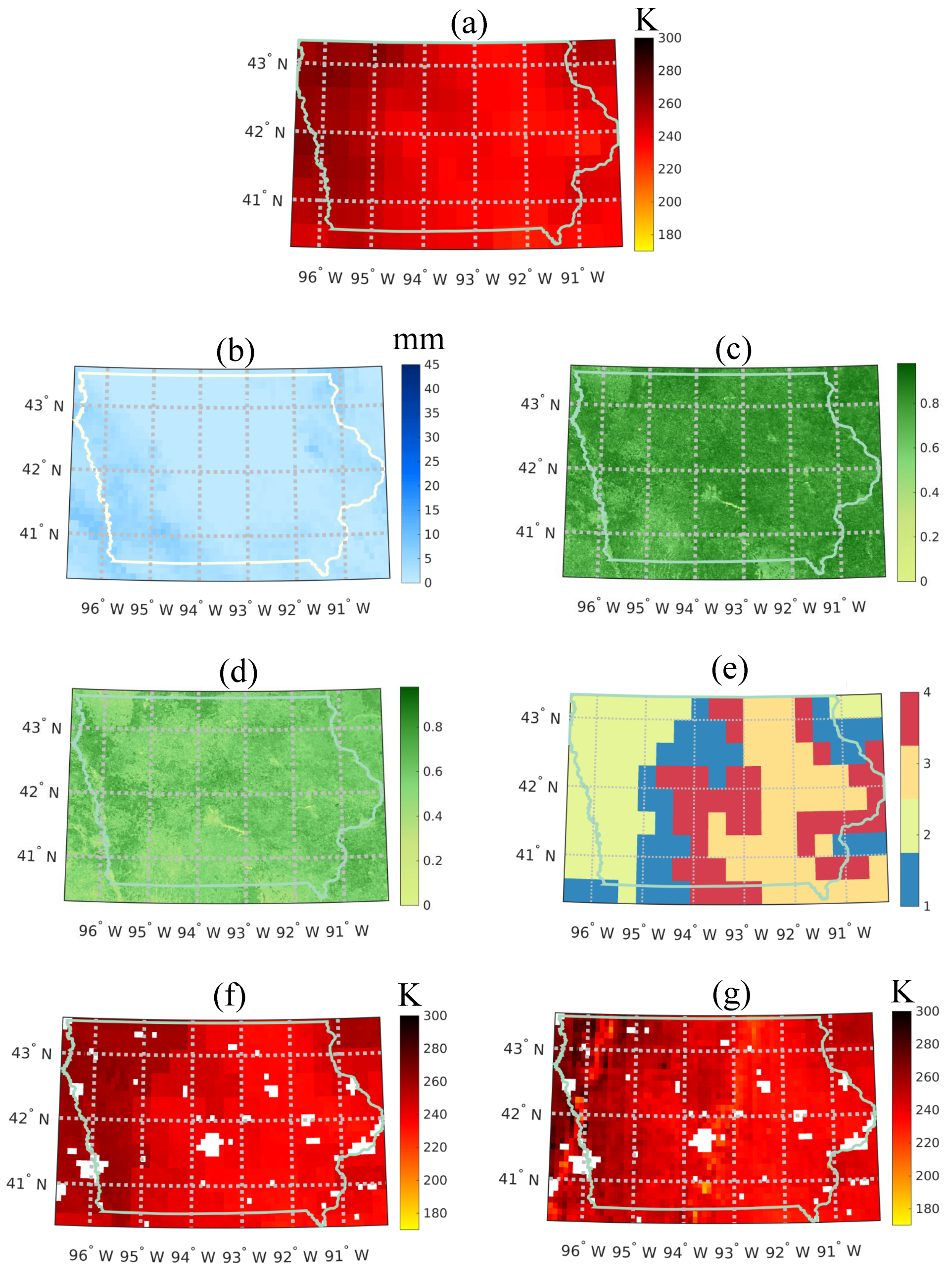

Fig. 7. DoY 181 - (a) SMAP L1C_TB product at 36km, (b) Precipitation at 1km, (c) Normalized Difference Vegetation Index at 1km, (d) Enhanced vegetation index at 1km, (e) Segmentation at 36km, (f) Disaggregated brightness temperature at 9km, (g) SMAP L3_SM_AP product at 9km.

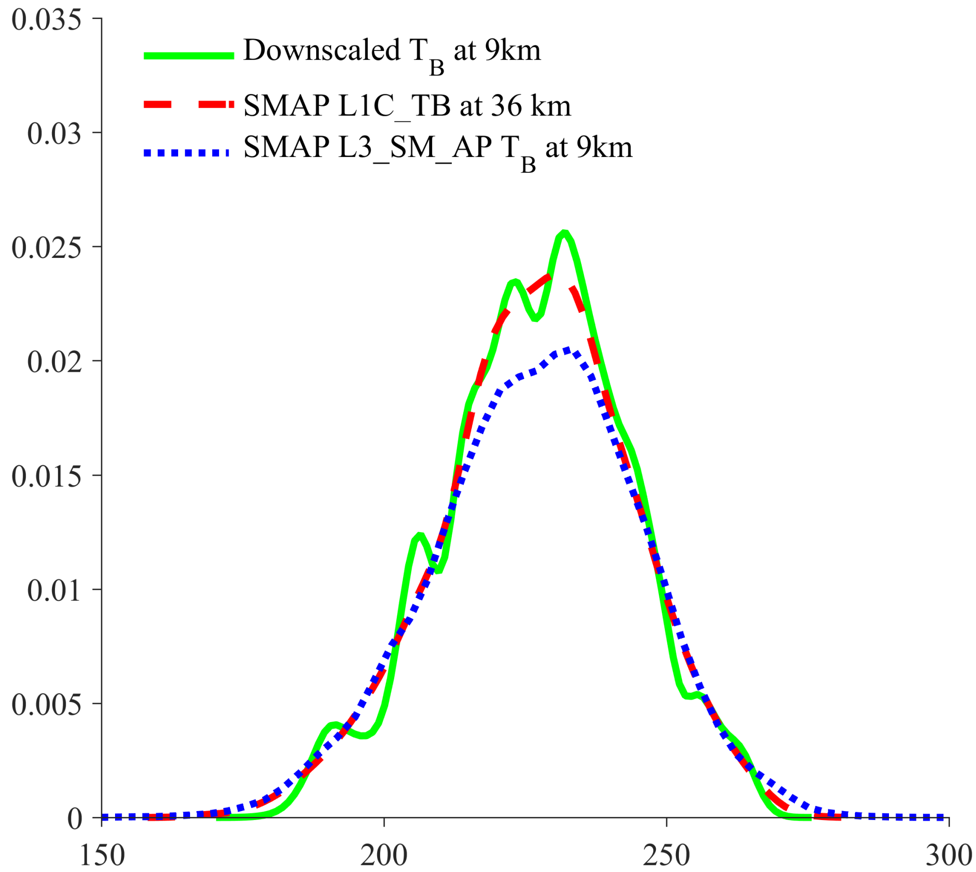

Fig. 8. Kernel density estimate of the probability density function (PDF) of SMAP L1C_TB product at 36km, SMAP L3_SM_AP product at 9km and Disaggregated brightness temperature at 9km,